

FINAL TECHNICAL REPORT
AWARD NUMBER: G15AP00028

Probabilistic Fault Displacement and Ground Deformation Hazard

Principal Investigator:

Dr Hong Kie Thio

Telephone number and email address:

AECOM Technical Services
300 S Grand Ave
Los Angeles, CA 90071

Start and End dates:

2015/01/01 – 2016/12/28

ABSTRACT

We have developed and applied a numerical method for ground deformation hazard for the Cascadia and Alaska subduction zones. The subsidence hazard analysis is part of the proposed revision of the ASCE 7 "Minimum Design Loads and Associated Criteria for Buildings and Other Structures" (ASCE, 2017) includes a chapter on "Tsunami Loads and Effects" (Thio et al., 2017), consists of maps of probabilistic subsidence for the coastal zones of Cascadia and Alaska. Our approach has allowed us to develop such a map in a manner that is fully consistent with the next version of the USGS National Earthquake Hazard Map, and will be published as part of the tsunami design chapter of ASCE 7-16 in late 2016/early 2017.

We also explored approaches for fault displacement hazard on a more localized (site-specific) scale, in particular given the limited amount of empirical data on surface rupture. The numerical approach provides the flexibility to study hazard for different parameters (e.g. displacement, uplift, strain) in a common framework. To this end, we have performed some exploratory numerical modeling of the ground deformation driven by slip on a buried rupture. These results clearly show the importance of soil structure and strength on the ground deformation at the surface.

1 Introduction

Probabilistic hazard analysis of ground deformation due to earthquake faulting is a relatively immature field, but has wide ranging applicability, not just in fault rupture hazard but also in general surface deformation hazard. The most common analysis is limited to offset along the fault, and to assess the deformation hazard away from the fault one needs to extrapolate the hazard from the fault using numerical or empirical means. Similarly, for tsunami hazard analysis it is desirable to use a probabilistic surface deformation model as input to tsunami hazard calculations. For complex fault ruptures or recurrence models, or buried faults, the probabilistic analysis needs to be carried out all the way to the ground deformation.

During this project, we have developed and applied a numerical method for ground deformation hazard for the Cascadia and Alaska subduction zones. The need for probabilistic uplift/subsidence hazard analysis is immediate as the proposed revision of the ASCE 7 "Minimum Design Loads and Associated Criteria for Buildings and Other Structures" (ASCE, 2017) includes a chapter on "Tsunami Loads and Effects" (Thio et al., 2017), and requires a map of probabilistic uplift/subsidence for the coastal zones of Cascadia and Alaska. Our approach has allowed us to develop such a map in a manner that is fully consistent with the next version of the USGS National Earthquake Hazard Map, and will be published as part of the tsunami design chapter of ASCE 7-16 in late 2016/early 2017.

We also believe that the numerical approach can help in developing approaches for fault displacement hazard on a more localized (site-specific) scale, in particular given the limited amount of empirical data on surface rupture. The numerical approach provides the flexibility to study hazard for different parameters (e.g. displacement, uplift, strain) in a common framework. Models of co-seismic slip distribution on faults have been developed in the last two decades, and several methods of generating stochastic models for earthquake slip, based on observed slip distributions (e.g Mai and Beroza, 2002), are now available. However, these models generally represent the slip in bedrock conditions at seismogenic depths since they are based on seismic observations. For surface deformation, we need to understand how seismogenic slip at depth is transferred to the surface through weaker upper layers. To this end, we have also performed some exploratory numerical modeling of the ground deformation driven by slip on a buried rupture. These results clearly show the importance of soil structure and strength on the ground deformation at the surface.

2 Surface Deformation Hazard Methodology

Probabilistic Ground Deformation Hazard is similar to the traditional PSHA in that it describes the behaviour of the ground due to earthquakes in particular site locations. Instead of a dynamical parameter such as ground acceleration, we are concerned with a static parameter such as uplift and subsidence. There is very limited empirical data for these parameters although this situation will change with the increasing availability of geodetic (GPS) and remote sensing (InSAR) data post-earthquake. Nevertheless, we can estimate the ground deformation hazard based on a probabilistic analysis of the fault displacement by using a hybrid approach combining probabilistic fault displacement hazard (e.g. Stepp et al., 2001; Youngs et al., 2003; Petersen et al., 2011) with numerical methods of computing ground deformation.

2.1 *Green's function summation*

Numerical algorithms that compute the static ground deformation from slip on a fault surface have proven to be very accurate, and are often used to invert the observed displacements into slip distributions on the fault. Linearity of the co-seismic ground deformation in bedrock also allows us to efficiently integrate over a large range of sources and magnitudes. The linearity implies that the displacement field of any rupture can be represented by a weighted summation of the displacement fields of smaller ruptures (Figure 1). Thus, by dividing a fault plane into smaller subfaults and pre-computing the displacement fields of small unit ruptures on every subfault we can express any deformation field from any arbitrary earthquake on the fault as a weighted summation (using the actual slip as weight) of the unit subfaults.

The integration over events is consistent with the one used for the PSHA, and the slip can be based on simple scaling relations of Wells and Coppersmith (1994), or the more comprehensive models of Petersen et al. (2011) or Youngs et al. (2003). However, the parameterization of the fault grids allows us also to use more sophisticated slip distribution based on a statistical analysis of published slip models (Somerville et al., 1999; Mai and Beroza, 2002). The efficiency of the Green's function summation technique allows us to integrate over thousands of scenarios if necessary in just a few hours or less.

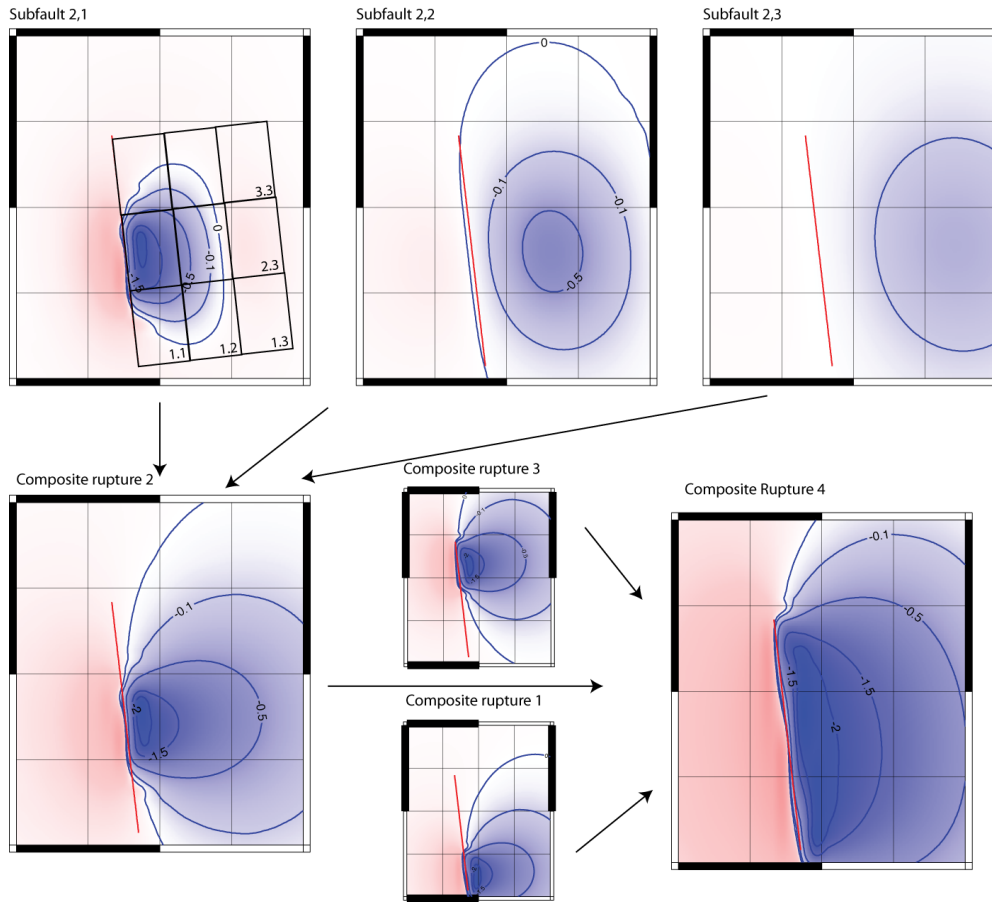


Figure 1. Rupture generation through subfault summation. In this example we have subdivided a WNW dipping normal fault into discrete elementary subfaults for which we compute the unit displacement field (displacement for 1 m slip on the subfault) at the surface. Because of the linearity of the static deformation, we can then compute the displacement field of any rupture on the fault as a summation of individual subfault displacement fields, weighted according to the actual slip on the fault, provided that the subfaults are chosen small enough to accommodate the rupture sampling interval of the PSHA and the minimum magnitude. Here, the subfault displacement fields from the center row (subfaults 2.1, 2.2 and 2.3) of the rupture are shown on the top, and summed to compute the displacement field for composite rupture (2, lower left), which represent an intermediate size earthquake. Similarly, we can model the entire rupture (lower right), i.e. the maximum earthquake size, by adding the remaining subfault ruptures. Note that for this example we have summed the subfault with unit weight, whereas in a real case we would have weighted the individual subfault contributions with the actual slip. Also, for the probabilistic analysis, a rupture is usually represented by several hundreds of subfaults, which allows for a comprehensive integration over the magnitude range and rupture locations.

Due to the linearity of the equations, we can transfer the aleatory uncertainties in the slip (i.e. the probabilistic fault displacement) directly into the ground displacement maps rather than having to integrate over a slip distribution function. Epistemic uncertainties are included in the usual way through logic trees.

We closely follow the formulation of the PSHA where we define the probability of ground deformation as follows:

$$v(z) = \sum_n v_n(z) \quad (1)$$

where $v_n(z)$ is the annual mean number (or rate) of events on source n for which Z , which is now subsidence, exceeds z at the site. The parameter $v_n(z)$ is given by the expression:

$$v_n(z) = \sum_i \sum_j \beta_n(m_i) \cdot p(R=r_j|m_i) \cdot p(Z>z|m_i, r_j) \quad (2)$$

where:

$\beta_n(m_i)$ = annual mean rate of recurrence of earthquakes of magnitude increment m_i on source n

$p(R_j|m_i)$ = probability that given the occurrence of an earthquake of magnitude m_i on source n , R represents the geometrical relation from the rupture surface to the site;

$p(Z > z|m_i, R_j)$ = probability that given an earthquake of magnitude m_i at a location R , the subsidence exceeds the specified level z .

2.2 Aleatory variability and epistemic uncertainty

2.2.1 Slip

The slip distribution on faults is not uniform, but shows a clear partition into areas of high slip (asperities) and low slip. The non-uniform slip distribution is an aleatory variability and can be included by summation over a large distribution of slip distributions that represent the same magnitude earthquake on a fault.

2.2.2 Numerical

The error in the actual computation of the ground deformation from a slip distribution at depth, given an elastic model of the crust, appears to be small. The main source of error is the use of an inappropriate crustal model – layered vs. half-space vs. 3D

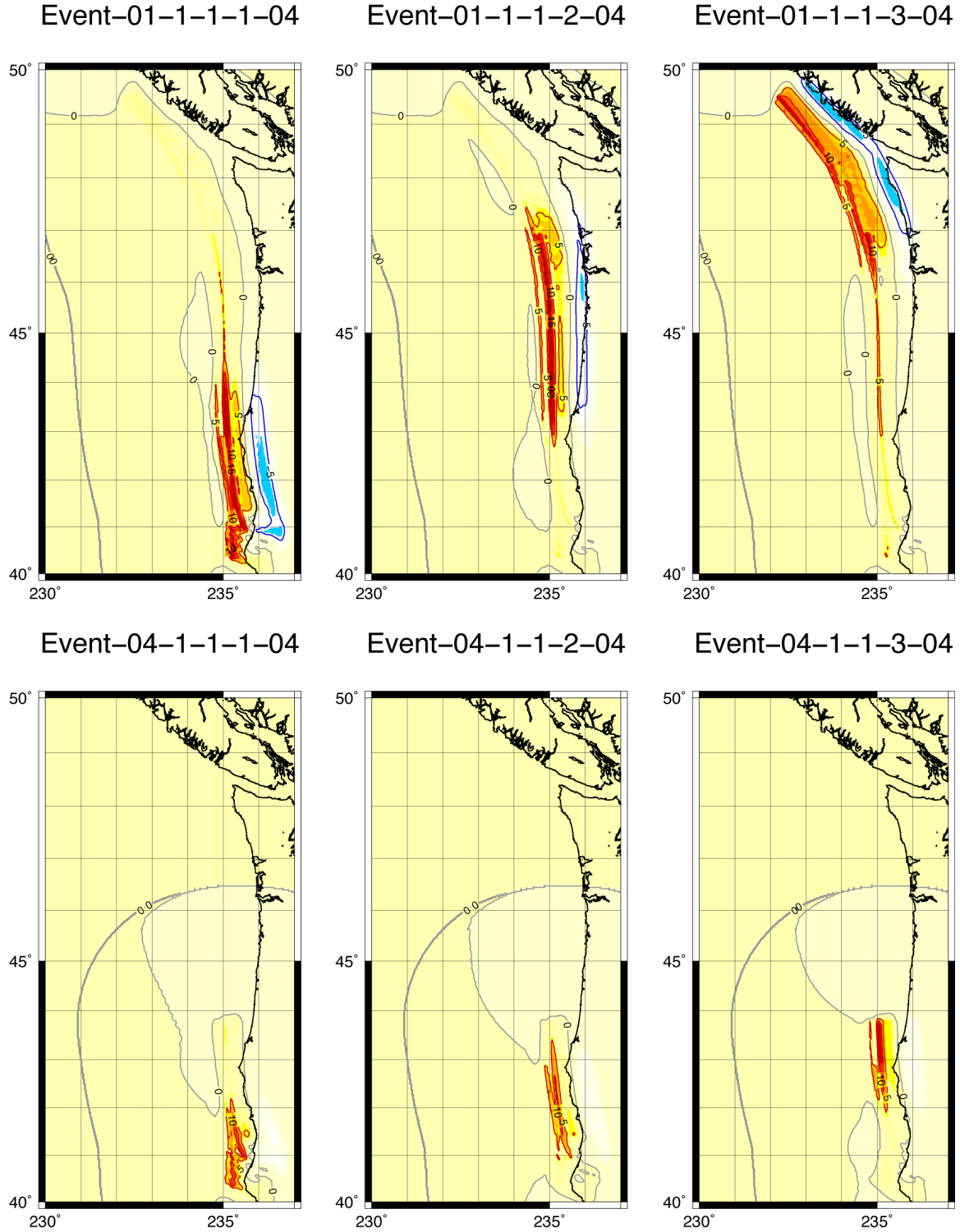


Figure 2. Multiple instances of two different size earthquakes. Top shows an M9 full rupture of the Cascadia subduction. The three instances are for a southern, central and northern asperity location respectively. Bottom shows the same for a M8.4 partial rupture.

The half-space approximation for computing surface deformation is often used due to the simplicity and availability of an analytical model for slip on a rectangular fault (Okada, 1985).

However, Savage (1989, 1998) demonstrated that using a half-space approximation gives relative large bias compared to a layered (1-D). The difference between 1-D and 3-D models (Wald and Graves, 2003) is much smaller, and we therefore used a 1-D FK method (Wang et al.,) to compute the static Green's functions to the surface.

Because of the much sharper dropoff of subsidence at larger distances, we can limit the summation in equation 2 to a much smaller set of sources than for the PSHA.

The term $p(Z > z|m_i, \mathbf{R}_i)$ is computed using the numerically predicted subsidence, which is the equivalent to the average or median ground motion level in PSHA, and a standard deviation σ which represents the combined aleatory uncertainty in the average slip as a function of magnitude and the uncertainty in subsidence as a function of slip on the fault. We have combined these terms together since the relationship between the slip and subsidence is linear.

As mentioned in the previous section, in lieu of an empirical model for subsidence we use a numerical approach to compute the subsidence as a function of slip on a rupture plane. Several methods for computing static deformation are available, and we computed the static displacement fields using a frequency-wave-number integration technique (FK) (Wang et al. 2003, 2006), which is commonly used in earthquake source modeling. This technique is preferable over the often-used analytical model of Okada (1985) because it computes the ground deformation using a layered crustal model rather than a half-space (Wald and Graves, 2001). In order to allow for a proper integration step we subdivided the rupture planes into elementary subfaults of 1x1 km or smaller and compute displacement Green's functions from every subfault to every point of a map grid. It may be preferable, especially if one is interested in strain rather than simple displacements, to use 3D Green's functions, in particular ones that include the effect of topography, since this may substantially change the strain components. Pitarka and Irikura (1996) developed a finite difference method, which includes topography as well as lateral variations in structure. Although this would require a much larger set of Green's functions, once computed for a particular area, these would again allow us to integrate efficiently over several thousands of scenarios.

Mapping errors, which are included in some of the PFDHA techniques, can be included by spreading the deformation according to distribution functions similar to the ones used in those methods if they can be regarded as epistemic uncertainties. For lateral aleatory variability, such as branching of the rupture plane, we can use simple numerical models to allow for generic branching of the fault, and distribute the deformation field along the fault. If branching occurs on well-defined strands, than it is straightforward to include those branches in the model directly.

2.3 Results

In Figure 2, we present several instances of two different-size earthquakes on the Cascadia subduction zone. Shown are the surface uplift and subsidence due to a slip distribution on the rupture plane, with red indicating uplift and blue subsidence. Given a certain earthquake in terms of fault length and width, which are obtained from a selected magnitude using scaling relations, we have developed several instances of the same basic earthquake with different slip distributions. In this case, because we are interested in large-scale deformation used for tsunami inundation modeling, we have chosen simple asperity models with maximum slip of

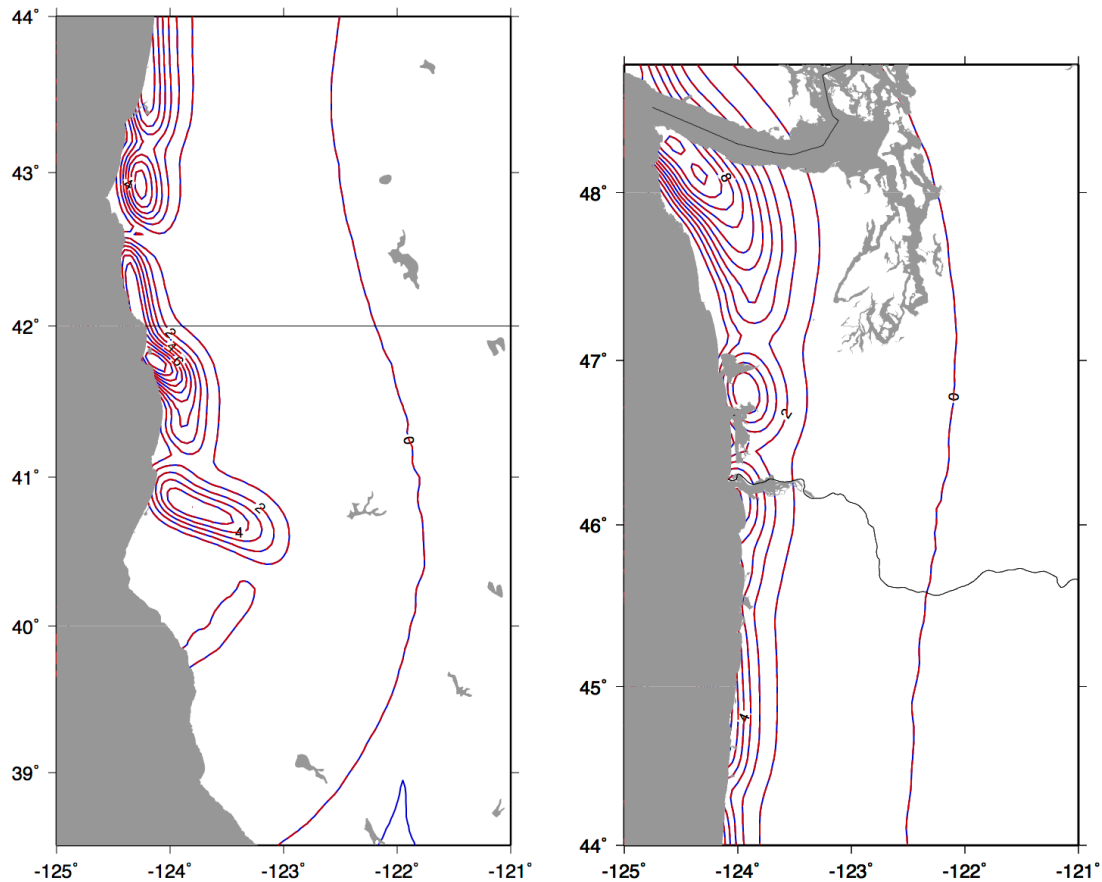


Figure 3. Probabilistic subsidence maps for the Cascadia region from the draft ASCE 7-16 tsunami design guidelines. The contours (every 2ft) are for the 2500 year average return period.

twice the average slip and asperities of one-third the size of the total rupture. However, for more site-specific cases, this simple scheme can be directly replaced with the results from stochastic rupture models. Using the simple asperity model, we have integrated over a large set of scenarios that represent the entire logic tree with branches for scaling relations, backstop depth, and other parameters. The final result is shown in Figure 3 where we present contours of exceedance subsidence for 2500 year (in ft) that will be included in the upcoming tsunami chapter of ASCE 7-16. Similar maps have also been computed for Alaska.

3 Surface Fault Displacement Hazard

The surface deformation response to deeper slip is relatively straightforward for large-scale patterns such as uplift and subsidence, as we have shown. For detailed, site-specific deformation, the issues are more complicated. Whereas faulting in bedrock can be relatively straightforward, the structure and geometry of the fault zone in the sedimentary overburden tend to be much more complex. Due to the lower strength of the overburden, rupture on a single fault at depth tends to become diffuse towards the free surface. In fact, soil deposits can prevent faulting from reaching the ground surface (e.g., Bray et al., 1994; Oettle et al., 2013), similar to blind thrust faults (Thio and Somerville, 2015), and otherwise cause

distributed folding of the ground surface separate from any discrete offset at the ground surface (Oettle and Bray, 2013a).

3.1 Methodology

Numerical modeling has been shown to accurately model the process of surface fault rupture through soil (Oettle and Bray, 2016). Therefore, a numerical modeling approach was selected herein to develop a preliminary set of soil correction factors. The numerical modeling methods of Oettle and Bray (2016) were largely adopted herein except that a different finite element code and constitutive model were employed.

The selected finite element code was PLAXIS 2D 2016 with a hardening constitutive model with small strain stiffness. Model parameters representative of a typical sandy soil were implemented as shown in Table 1. These modeling parameters resulted in an axial soil failure strain in anisotropic triaxial compression at 100 kPa initial vertical stress of about 4%.

Table 1. Constitutive model parameters used in the subject analyses.

Model Parameter	Value
Drainage Type	Drained
Unit Weight	20 kN/m ³
E_{50}^{ref}	15,000 kN/m ²
E_{oed}^{ref}	18,000 kN/m ²
E_{ur}^{ref}	55,000 kN/m ²
Power (m)	0.5
c'_{ref}	0 kN/m ²
ϕ'	30°
ψ	0°
$\gamma_{0.7}$	0.00015
G_0^{ref}	80,000 kN/m ²
v'_{ur}	0.2
P_{ref}	100 kN/m ²
K_0^{nc}	0.45
c'_{inc}	0 kN/m ²
y_{ref}	0 m
R_f	0.9
Tension Cutoff	0 kN/m ²

K_0^{int}	0.45
OCR^{int}	1.0

The soil was modeled as virgin soil, e.g., without modeling stress changes or a damage zone resulting from previous fault ruptures (Oettle and Bray, 2013a). This was done to simplify the proof-of-concept model and to make the model applicable to recently deposited soil or fill. Finite element analyses were conducted pseudostatically, which has been shown to be a reasonable modeling method for surface fault rupture models (Oettle et al., 2015).

A series of five (5) simulations were conducted with the thickness of the overburden soil over a basement rock varied in each analysis. Soil depths of 5 m, 10 m, 15 m, 20 m, and 30 m were used. A 60° dip reverse fault was used for all analyses to facilitate comparison of the results to isolate the effect of overburden soil thickness. To interpret the modeling results, each model was conducted in two phases after the initial stress initialization: (1) an initial phase of fault displacement of a magnitude necessary to generate a shear band from the base fault through to the ground surface, and (2) after resetting the displacements within the finite element model, the remainder of the faulting necessary to reach a total vertical rock offset of 0.87 m (equivalent to 1 m when measured along the dip of the fault). The breakdown of the fault displacement into two phases is meant to ease interpretation of the results, as shown subsequently.

The main parameter of interest for these analyses was the discrete fault offset at the ground surface (y_{soil}) compared to the basement displacement in the underlying rock (y_{rock}). These displacements were measured herein in the vertical direction, i.e., not in the along fault direction, to facilitate interpretation, as shown in Figure 4.

The discrete fault offset at the ground surface was measured from the numerical model by counting the displacement that occurred over the five adjacent elements which would result in the highest measured displacement, as shown in Figure 4. This assumption for offset measurement was necessary because the finite element model did not directly output movement along a shear band, as the model does not include strain softening or embedded strong discontinuities.

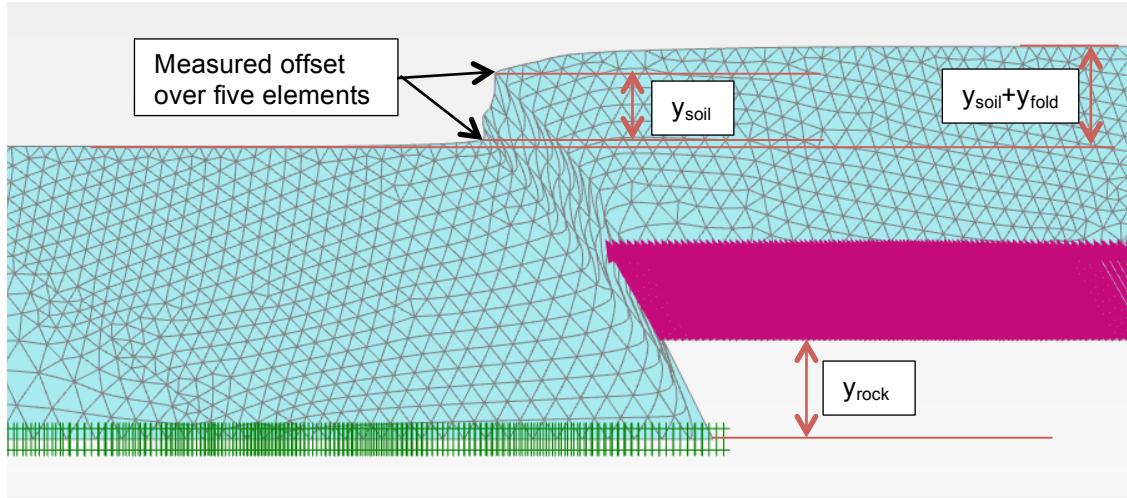


Figure 4. Measurements made in the finite element model for determining discrete surface offset.

3.2 Results

The results of the five simulations are presented in Figure 5, where the resulting $y_{\text{soil}}/y_{\text{rock}}$ is presented as a function of the overburden thickness. The ratio $y_{\text{soil}}/y_{\text{rock}}$ represents the discrete vertical soil offset at the ground surface in Phase 5 of the simulation normalized by the total basement rock vertical offset in Phase 1 and Phase 2 (which was held constant at 0.87 m herein).

Several recommendations are presented here for future research consideration:

1. Widening application of the subject methodology to other fault types, fault dips, displacement magnitudes, and soil conditions. It is anticipated that significant normalizing of the applicable parameters can be achieved to estimate discrete surface offsets from a limited set of input parameters (such as soil thickness and soil failure strain).
2. Studying the effect that previous fault ruptures will have on subsequent fault ruptures through the same soil. It is likely that pre-existing stress conditions and damage zones will result in greater localized shear zones at the ground surface (Oettle and Bray, 2013a).
3. Studying the numerical aspects of strain softening and strain localization on discrete discontinuities and how those numerical techniques would affect the results. Specifically, to refine the method used herein of using the offset measured over five adjacent elements as the “discrete” surface offset.
4. A comprehensive comparison of numerically predicted $y_{\text{soil}}/y_{\text{rock}}$ compared to field data, and an assessment of the uncertainty associated with estimating $y_{\text{soil}}/y_{\text{rock}}$.

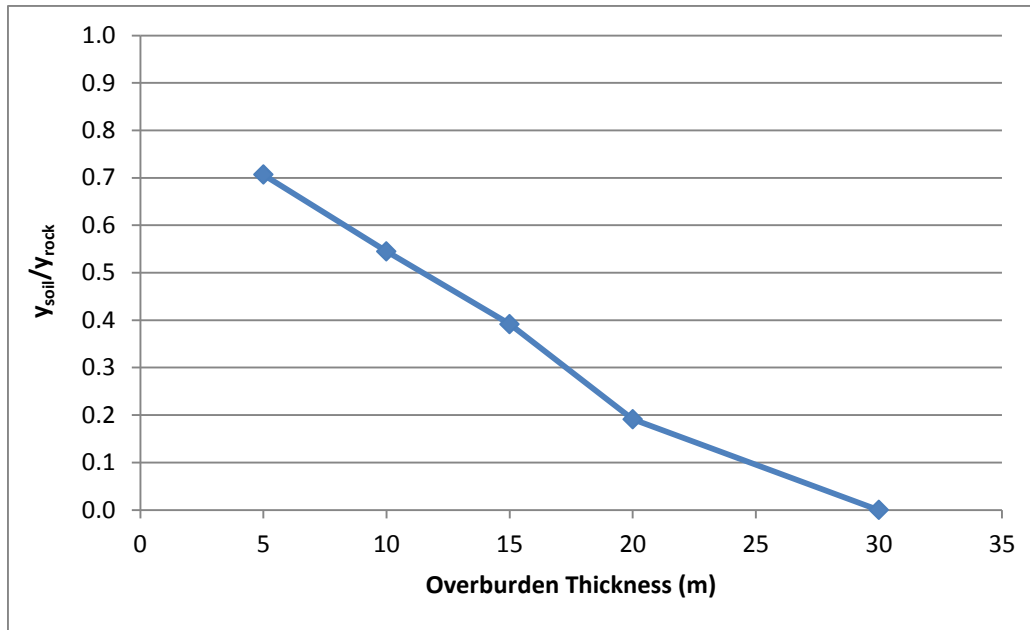


Figure 5. Results of the five analyses showing the ratio of surface fault vertical offset to the basement rock vertical fault offset as a function of soil overburden thickness.

4 References

- Abrahamson, N., 2008, Appendix C Probabilistic Fault Rupture Hazard Analysis: San Francisco PUC, General Seismic Requirements for the Design on New Facilities and Upgrade of Existing Facilities, 1–7 p.
- American Society of Civil Engineers (ASCE), 2017. Minimum Design Loads For Buildings and Other Structures, ASCE 7-16,
- Coppersmith, K.J., and Youngs, R.R., 2000, Data needs for probabilistic fault displacement hazard analysis: *Journal of Geodynamics*, v. 29, no. 3, p. 329–343.
- Mai, M., Beroza, G. (2002), A Spatial Random Field Model To Characterize Complexity In Earthquake Slip. *J Geophys Res* 107, B11
- Moss, R. E. S. and Z. Ross, 2011. Probabilistic Fault Displacement Hazard Analysis for Reverse Faults. *Bull. Seismol. Soc. of Am.*, 101(4).
- Moss, R. E. S. and T. Travararou, 2006. Tsunamigenic Probabilistic Fault Displacement Hazard Analysis For Subduction Zones, 8th National Conference on Earthquake Engineering, 1906 San Francisco Earthquake 100th Anniversary
- Oettle, N.K., and Bray, J.D. (2013a). "Fault rupture propagation through previously ruptured soil." *Journal of Geotechnical and Geoenvironmental Engineering*, in press.
- Oettle, N.K. and Bray, J.D. (2013b). "Geotechnical Mitigation Strategies for Earthquake Surface Fault Rupture." *Journal of Geotechnical and Geoenvironmental Engineering*, 139:11, 1864–1874.
- Oettle, N.K., and Bray, J.D., (2016). "Numerical Procedures for Simulating Earthquake Fault Rupture Propagation". *International Journal of Geomechanics*, In Press.
- Oettle, N.K., Bray, J.D., Konagai, K., and Kelson, K. (2013). "Surface Fault Rupture through a Ridge in an Aftershock of the 2011 Tohoku Earthquake." *2013 Geo-Congress*.

- Oettle, N.K., Bray, J.D., and Dreger, D.S. (2015). "Dynamic Effects of Surface Fault Rupture Interaction with Structures." *Soil Dynamics and Earthquake Engineering*, 72, 37–47.
- Okada, Y., 1985. Surface deformation due to shear and tensile faults in a half-space, *Bull. Seism. Soc. Am.*, 75, 1135-1154.
- Petersen, M.D., T. E. Dawson, R. Chen, T. Cao, C. J. Wills, D. P. Schwartz, and A. D. Frankel, 2011, Fault Displacement Hazard for Strike-Slip Faults, *Bull. of the Seismol. Soc. of Am.*, 101, 805 - 825.
- Pitarka, A. and K. Irikura : Modeling 3D surface topography by finite-difference method: Kobe-JMA station site, Japan, case study, *Geophys. Res. Lett.*, 23, 2729-2732, 1996.
- Ross, Z.E., 2011, PROBABILISTIC FAULT DISPLACEMENT HAZARD ANALYSIS FOR REVERSE FAULTS AND SURFACE RUPTURE SCALE INVARIANCE:
- Somerville, P., Irikura, K., Graves, R., Sawada, S., Wald, D., Abrahamson, N., Iwasaki, Y., Kagawa, T., Smith, N., Kowada, A. (1999), Characterizing Crustal Earthquake Slip Models For The Prediction Of Strong Ground Motion. *Seismol Res Lett* 70, 199–222
- Stepp, J.C., I. Wong, J. Whitney, R. Quittmeyer, N. Abrahamson, G. Toro, R. Youngs, K. Coppersmith, J. Savy, T. Sullivan, and Y. M. P. P. Members, 2001. Probabilistic Seismic Hazard Analyses for Ground Motions and Fault Displacement at Yucca Mountain, Nevada. *Earthquake Spectra*, 17, 113–151.
- Thio, H.K., Somerville, P., and J. Polet, 2010. Probabilistic Tsunami Hazard in California, Report to the Pacific Earthquake Engineering research Center, Berkeley, CA. http://peer.berkeley.edu/publications/peer_reports/reports_2010/web_PEER2010_108_THIOetal.pdf
- Thio, H.K., and Somerville, P.G., (2015). "Applications of probabilistic ground deformation hazard." In: *10th Pacific Conference on Earthquake Engineering*.
- Thio, H.K., Wei, Y., Li, W., And Chock, G., (2017): Development Of Offshore Probabilistic Tsunami Exceedance Amplitudes For Asce 7-16, 16th World Conference On Earthquake Engineering, 16wcee 2017, Santiago, Chile.
- Wald, D. J., and R.W. Graves (2001). Resolution Analysis of Finite Fault Source Inversion Using 1D and 3D Green's Functions, Part II: Combining Seismic and Geodetic Data, *J. Geophys. Res.*, 106, 8767.
- Wang, R, F. Lorenzo-Martín and F. Roth, 2003. Computation of deformation induced by earthquakes in a multi-layered elastic crust—FORTRAN programs EDGRN/EDCMP, *Computers & Geosciences*, 29, 195–207.
- Wang, R, F. Lorenzo-Martín and F. Roth, 2006. Erratum to: "Computation of deformation induced by earthquakes in a multi-layered elastic crust—FORTRAN programs EDGRN/EDCMP", *Computers & Geosciences*, 32, 1817.
- Wells, D.L., and K.J. Coppersmith, New empirical relationships among magnitude, rupture length, rupture width, rupture area, and surface displacement, *Bulletin of the Seismological Society of America*, 84 (4), 974-1002, 1994.
- Youngs, R.R., W. J. Arabasz, R. E. Anderson, A. R. Ramelli, J. P. Ake, D. B. Slemmons, J. P. McCalpin, D. I. Doser, C. J. Fridrich, F. H. Swan, III, A. M. Rogers, J. C. Yount, L. W. Anderson, K. D. Smith, R. L. Bruhn, P. L. K. Knuepfer, R. B. Smith, C. M. dePolo, D. W. O'Leary, K. J. Coppersmith, S. K. Pezzopane, D. P. Schwartz, J. W. Whitney, S. S. Olig, and G. R. Toro, 2003. A Methodology for Probabilistic Fault Displacement Hazard Analysis (PFDHA), *Earthquake Spectra* 19, pp. 191-219; doi:10.1193/1.1542891

